Solubility of Nitrogen and Inclusion Characteristics in High Aluminium Steels

Mir Ishfaq[1] and Manish M Pande[*1]

Department of Metallurgical Engineering and Materials Science

Indian Institute of Technology Bombay, Mumbai, Pin 400076, Maharashtra, India,

Phone no. 022 25767609

*Corresponding author: manish.pande@iitb.ac.in

Abstract

The effect of aluminium on nitrogen solubility was investigated by equilibrating melt comprising master alloy of Fe-Al with pure electrolytic iron in a controlled atmosphere (pure argon) at 1873 K. Nitrogen in the samples was measured by sampling technique using inert gas fusion absorptiometry. It was found that nitrogen content decreases steadily with aluminium concentration and gradually, becomes close to 1 ppm for very high aluminium steels. Wagner's second order interaction parameter formalism has been used to estimate the equilibrium constant and interaction parameters. Scanning electron microscopy (SEM) investigation showed, dual-phase inclusions comprising AlN phase surrounding alumina core. The 3-D morphology of inclusions was studied by extracting the sample from the top and the central bottom portion of the solidified ingot. A sparse distribution of nitrogen was found for most of the inclusions which manifested the presence of almost pure alumina inclusions with different morphologies and sizes.

Keywords: Nitrogen solubility, High aluminium steels, Interaction parameters, Dual-phase inclusions.

1. Introduction

Solubility of nitrogen in very high aluminium steels has been rarely studied so far. During secondary steelmaking, most of the focus is on removal of oxygen by adding aluminium wire and minimizing the unwanted impurities like alumina inclusions and sulphur by adding lime to the melt. However, nitrogen dissolution in steels also impact the properties of the metal. The

nitrogen dissolution in steels happens as per Sievert's law where molecular nitrogen dissociates into atomic nitrogen as shown in **Eq. (1)** and **Eq. (2)** (Sieverts, 1935).

$$\frac{1}{2}\mathrm{N}_2(\mathrm{g}) = \underline{\mathrm{N}} \quad (1)$$

$$\Delta \mathrm{G}^\circ = -RT \ln K = 3{,}598 + 23.89\ \mathrm{T}\ \mathrm{J/mole}\ \text{(Turkdogan, 1980)} \quad (2)$$

The affinity of nitrogen towards metals especially aluminium is lower as compared to that of oxygen towards aluminium due to difference in electronegativity. However, aluminium is known to form a stable nitride in steels (Hsiao, 1958). Both aluminium nitride and alumina inclusions have detrimental effects on the mechanical properties of the steel and hence both are undesirable. It is therefore crucial to study the evolution of their morphology, size, and growth. Presence of nitrogen however in steels can appreciably enhance interstitial solid solution strengthening. Nitrogen occupies an interstitial site and can lock the movement of dislocations. Examining the solubility of nitrogen is crucial, similar to investigating the solubility of oxygen, in relation to varying concentrations of aluminum as nitrogen plays a significant role in determining the physical and mechanical properties of metal after solidification. During solidification, excess nitrogen can come out as bubbles thus causing solidification defects like blowholes in metal. Some nitrogen may react with alloying elements like aluminium and form nitrides. The remaining nitrogen stays in the interstitial sites promoting austenitic (γ) structure. Nitrogen, similar to oxygen, exists in two forms: the soluble nitrogen which occupies interstitial sites and the insoluble nitrogen that forms nitride inclusions.

Most of the researchers have investigated the solubility of nitrogen in low aluminium steels at different partial pressures of nitrogen and have determined nitrogen either by using Sievert's method or sampling technique. A substantial work has been carried out in determining the solubility of nitrogen in liquid iron containing different alloying elements (Pehlke and Elliott, 1960; Wada and Pehlke, 1977; Ishii, Ban-ya and Fuwa, 1982; Kim *et al*, 2007; Paek *et al*, 2013) at different partial pressures of nitrogen. In the present work, the prime focus is on the effect of aluminium on the dissolved nitrogen using sampling method. At aluminium concentration > 5 wt.%, there is hardly any reported data on the solubility of nitrogen in Fe-Al alloy. Sievert's method is based on gas solubility in molten metal at a particular gas pressure while in sampling method, the analysis of nitrogen is done after analyzing the solidified metal. The analysis of nitrogen involves various methods, for example, using either Kjeldahl method or using inert gas fusion method. Beeghly *et al* (1949) determined nitrogen from aluminium nitride present

in aluminium killed Bessemer steel and open-hearth steel using micro-Kjeldahal method. Kim *et al* (2007) studied the thermodynamics of AlN formation at various nitrogen partial pressures. Nitrogen solubility in high manganese, high aluminium steels was investigated by Paek *et al* (2013) at varying partial pressures of nitrogen (0.1-0.8 atm). Both used inert gas fusion method for determination of nitrogen and oxygen in the samples. Nitrogen content in the previous work was in the range of several hundred to even thousands of ppm however in the present work, it was limited in the range of 17 ppm (initial) to less than a ppm (final).

2. Experimental Methodology

Electrolytic iron chunks (weighing around 60-90 grams) along with Fe-Al master alloy were melted in the pure alumina crucible (99.99% pure) at 1873 K using a vertical tube furnace (Carbolite Gero) as shown in **Figure 1**. The temperature, heating rate, cooling rate and dwelling time was set by a Nanodac controller. Detailed experimental procedure can be found in our previous work (Mir and Pande, 2024). The equilibration time of 2 h was provided for the melt. The sample underwent heating, melting, and cooling in the furnace in an inert (purified argon) atmosphere. Analysis of aluminium and nitrogen was conducted on samples extracted from the central bottom (CB) portion of the ingot. The thickness of CB region was 1 cm and it was sliced away from the bottom most region (thickness 0.5 cm), as shown in **Figure 2**. The quantitative determination of aluminium content was carried out using Inductively Coupled Plasma-Atomic Emission spectroscopy (ICP-AES, SPECTRO ARCOS). In the CB region, two cuboidal samples (4 mm×5 mm×8 mm) each with a mass of ~1 gram were taken for the nitrogen analysis using inert gas fusion infrared absorptiometry (LECO ON-736).

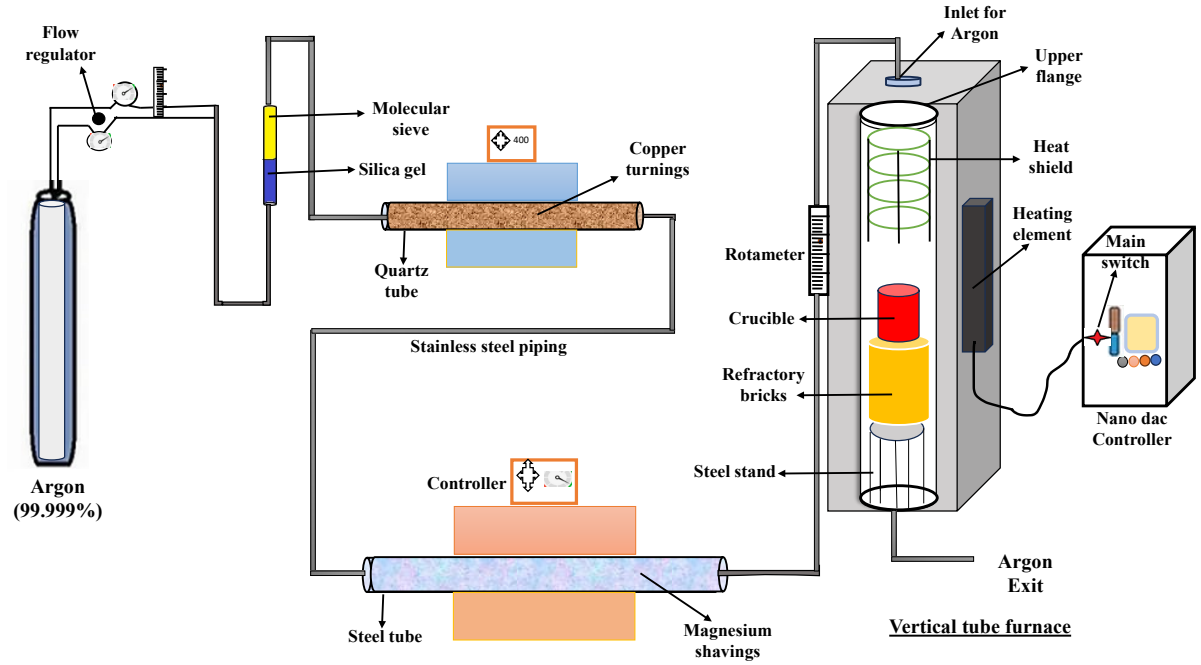

Figure 1 - Schematic of the high temperature experimental set-up

Initial nitrogen (melted electrolytic iron) was in the range of 46-50 ppm. Prior to melting, the total oxygen was found to be in the range of 93 to 115 ppm with accuracy of $\pm$ 4 ppm in the electrolytic iron flakes using LECO. while the total oxygen measured in the solidified samples (after melting in the furnace without any addition) was in the range of 100-120 ppm. For nitrogen analysis, the average of the two samples from the central bottom region of the solidified ingot was considered. However, for inclusion analysis, samples were taken from the top portion and CB region. These samples were examined using environmental scanning electron microscope (ESEM-FEI Quanta 200) for inclusion characteristics. For investigating the 3-D morphology of inclusions, the sliced portion from the top and CB portion of ingot was dissolved in HCl (dilute 1:1 v/v). The filtrate was allowed to remain on Whatman filter paper with a pore size of 2.5 microns. The residue was then dried and placed over the carbon tape. Platinum coating was applied over it, and the inclusions were analysed using the SEM in secondary electron (SE) mode. The morphology, size, and elemental mapping of the inclusions were investigated and are elaborated in the 'Results and discussion' section. The detailed sampling methodology is depicted in **Figure 2**.

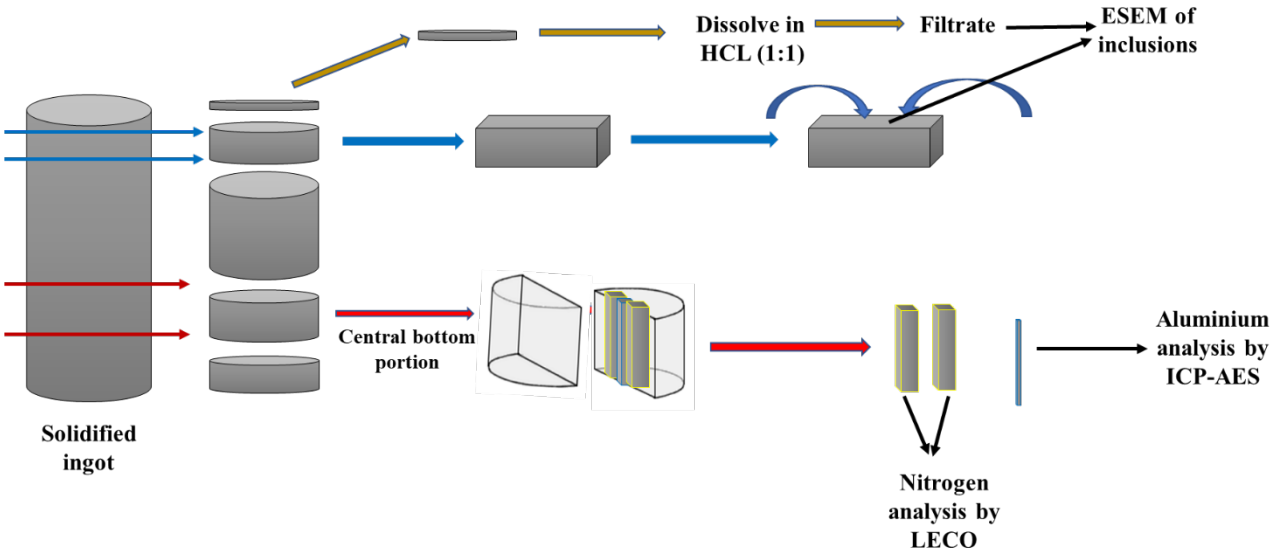

Figure 2 - Sampling Methodology

3. Results and discussion

The nitrogen content in the present experiments was limited as the high temperature experiments were carried out in a high-purity argon atmosphere rather than maintaining nitrogen at various partial pressures. This gives an important advantage of determining solubility of nitrogen in an inert atmosphere and therefore, formation of a fine deposit of aluminium nitride over the melt surface is prevented at higher aluminium concentration. The vapor pressure of aluminium at 1873 K is 182 pascals which is much more than that of liquid iron. In nitrogen atmosphere, some portion of vaporized aluminium may react with nitrogen present in the surrounding atmosphere and form a stable nitride layer or deposit over the melt surface (Pehlke and Elliott, 1960; Kim *et al*, 2007). In the present study, Al-N data from the selected experiments was considered as shown in **Table 1**. Al concentration range was much wider as compared to the nitrogen range. While establishing the equilibrium between aluminum and oxygen (Al-O), the oxygen concentration exhibited rapid fluctuations even with minor changes in aluminum concentration (Kang et al., 2009; Paek et al., 2015; Mir and Pande, 2024). However, in assessing nitrogen solubility in the current experiments across varying aluminum concentrations, there was no discernible change in nitrogen concentration for the initial 10 experiments outlined in Table 1. Moreover, considering the narrow nitrogen concentration range and calibration of nitrogen against a standard within $\pm$ 3 ppm, resulted in the minimal variation in a N content for the increasing Al concentrations.

Table 1 - Equilibrium concentration of Al and N in steel measured after solidifying the samples

wt.% Al	**Nitrogen in wt.% (±3 ppm)**
0.0735	0.00162
0.14	0.001685
0.256	0.001925
0.279	0.001763
0.519	0.002445
1.132	0.00213
1.386	0.001575
1.704	0.00205
5.462	0.001555
5.985	0.001648
8.375	0.000133
9.518	0.000065
11.78	0.000089
13.013	0.000121
15.097	0.000095
21.56	0.000118
23.35	0.000057

As the aluminium content in the sample increases beyond a certain critical concentration, the dissolved nitrogen decreases. The change in nitrogen content is not prominent in the beginning as the nitrogen concentration fluctuates between 24 to 15 ppm. However, the trend was quite dissimilar to that of Al-O equilibria where oxygen was minimum in the certain concentration range of aluminium (Kang *et al*, 2009; Paek *et al*, 2015; Mir and Pande, 2024). Beyond a particular concentration of aluminium, the oxygen started to increase again. It should be

mentioned here that Kim *et al* (2007) found similar behavior of decrease in nitrogen with increase in aluminium content in their experiments. In the present work, the nitrogen content was close to 1 ppm in all the samples when aluminium content was more than 8.375 wt.%. Interestingly Ishii *et al* (1982) and Paek *et al* (2013) found out a contrasting feature with addition of manganese. In their experiments, addition of manganese increased the solubility of nitrogen.

3. (a) Thermodynamic assessment of aluminium nitrogen

The thermodynamics of Fe-Al-N system can be assessed by considering Al and N as two solutes dissolved in solvent iron. It is important to consider iron and aluminium along with O or N while considering the thermodynamics of ternary system. In the present study, Fe-Al-O and Fe-Al-N ternary systems can be separately considered instead of a quaternary Fe-Al-O-N system because it is unlikely that nitrogen and oxygen would contribute to any mutual interaction. Thermodynamics of Fe-Al-O ternary system has been already elucidated in our previous work using different formalisms (Mir and Pande, 2024). For Fe-Al-N system, the formation of aluminium nitride has been considered by the following reaction

$$\underline{\mathrm{Al}} + \underline{\mathrm{N}} = \mathrm{AlN} \tag{3}$$

The equilibrium constant for the above reaction can be written as

$$K_1 = \frac{a_{AlN}}{a_N a_{Al}} \tag{4}$$

The Henrian activity of component j (relative to 1 mass %) can be written as the product of activity coefficient (f_i) and wt.% j

Considering AlN as pure, the activity of AlN can be taken as unity. Further, the Henrian activity of component 'j' relative to the hypothetical 1 mass% standard in liquid iron can be taken as the product of activity coefficient (f_j) and weight percent of component j (wt. % j). Expanding **Eq. (4)**,

$$\log(f_N) + \log(\text{wt.\%N}) + \log(f_{Al}) + \log(\text{wt.\%Al}) = \log \frac{1}{K_1} \tag{5}$$

Considering the Wagner's 2nd order interaction parameter formalism (WIPF 2nd order) for expansion of $\log(f_N)$ and $\log(f_{Al})$ (ignoring the 3rd and higher order ones),

$$e_{Al}^{Al}(wt.\%Al) + e_{Al}^{N}(wt.\%N) + r_{Al}^{Al}\,(wt.\%Al)^2 + r_{Al}^{N}\,(wt.\%N)^2 + r_{Al}^{Al,N}\,(wt.\%Al)(wt.\%N) + \log(wt.\%Al) + e_{N}^{Al}(wt.\%Al) + e_{N}^{N}(wt.\%N) + \log(wt.\%N) + r_{N}^{N}\,(wt.\%N)^2 + r_{N}^{Al}\,(wt.\%Al)^2 + r_{N}^{Al,N}(wt.\%Al)(wt.\%N) = \log K \quad (6)$$

Where K is the inverse of K_1

Taking atomic weights of Fe, Al and N as 55.85, 27 and 14 respectively, the relationship between different interaction parameters (Lupis relationship) can be obtained as follows (Lupis, 1983)

$$e_{Al}^{(N)} = 1.92856\, e_{N}^{(Al)} - 4.0373 \times 10^{-3} \quad (7)$$

$$r_{Al}^{(Al,N)} = 3.857\, r_{N}^{(Al)} - 0.0192856\, e_{N}^{(Al)} + 0.01\, e_{Al}^{(Al)} \quad (8)$$

$$r_{N}^{(Al,N)} = 1.037\, r_{Al}^{(N)} - 0.01\, e_{N}^{(Al)} + 0.01\, e_{N}^{(N)} - 2.0933 \times 10^{-5} \quad (9)$$

The values of self-1st and 2nd order interaction parameters e_{N}^{N} and r_{N}^{N} have been taken as 0 (Sieverts and Zapf, 1935). The values of e_{Al}^{Al} and r_{Al}^{Al} have been taken as 0.045 and -0.001 (Sigworth and Elliott, 1974).

Substituting **Eq. (7)**, **(8)** and **(9)** in Eq. **(6),**

$$0.045(wt.\%Al) + \left[1.92856\, e_{N}^{(Al)} - 4.0373 \times 10^{-3}\right](wt.\%N) - 0.001\,(wt.\%Al)^2 + r_{Al}^{N}\,(wt.\%N)^2 + \left[3.857\, r_{N}^{(Al)} - 0.0192856\, e_{N}^{(Al)} + 0.01\, e_{Al}^{(Al)}\right](wt.\%Al)(wt.\%N) + \log(wt.\%Al) + e_{N}^{Al}(wt.\%Al) + \log(wt.\%N) + r_{N}^{Al}\,(wt.\%Al)^2 + \left[1.037\, r_{Al}^{(N)} - 0.01\, e_{N}^{(Al)} + 0.01\, e_{N}^{(N)} - 2.09332 \times 10^{-5}\right](wt.\%Al)(wt.\%N) = \log K \quad (10)$$

Rearrangement of **Eq. (10)** gives

$$0.045(wt.\%Al) - 4.0373 \times 10^{-3}(wt.\%N) - 0.001\,(wt.\%Al)^2 + \log(wt.\%Al) + \log(wt.\%N) + 4.29067 \times 10^{-4}(wt.\%Al)(wt.\%N) = e_{N}^{(Al)}[-1.92857(wt.\%N) + 0.0292856\,(wt.\%Al)(wt.\%N) - (wt.\%Al)] + r_{N}^{Al}[-3.857\,(wt.\%Al)(wt.\%N) - (wt.\%Al)^2] + r_{Al}^{N}[-1.037\,(wt.\%Al)(wt.\%N) - (wt.\%N)^2] + \log K \quad (11)$$

For determining the values of interaction parameters ($e_{N}^{(Al)}$, r_{N}^{Al} and r_{Al}^{N}) and equilibrium constant ($\log K$), **Eq. (11)** can be represented by the form

$$y = \lambda_1 x_1 + \lambda_2 x_2 + \lambda_3 x_3 + C$$

Where, $y = 0.045(\text{wt.}\%\text{Al}) - 4.0373 \times 10^{-3}(\text{wt.}\%\text{N}) - 0.001\ (\text{wt.}\%\text{Al})^2 + \log(\text{wt.}\%\text{Al}) + \log(\text{wt.}\%\text{N}) + 4.29067 \times 10^{-4}(\text{wt.}\%\text{Al})(\text{wt.}\%\text{N})$

$x_1 = -1.92857(\text{wt.}\%\text{N}) + 0.0292856\ (\text{wt.}\%\text{Al})(\text{wt.}\%\text{N}) - (\text{wt.}\%\text{Al})$

$x_2 = -3.857\ (\text{wt.}\%\text{Al})(\text{wt.}\%\text{N}) - (\text{wt.}\%\text{Al})^2$

$x_3 = -1.037\ (\text{wt.}\%\text{Al})(\text{wt.}\%\text{N}) - (\text{wt.}\%\text{N})^2$

$\lambda_1, \lambda_2, \lambda_3$ and C represent $\mathrm{e}_{\mathrm{N}}^{(\mathrm{Al})}$, $\mathrm{r}_{\mathrm{N}}^{\mathrm{Al}}$, $\mathrm{r}_{\mathrm{Al}}^{\mathrm{N}}$ and $\log K$ respectively

Based on the present experimental data as compiled in **Table 1**, the values of all the unknowns in **Eq. (11)** have been estimated using multiple linear regression. The value of R^2 was found to be 0.83. The plot on log scale is shown in **Figure 3**. The values of unknowns obtained on regression analysis are given as below:

Intercept $= \log K = -3.355 \pm 0.114$

$\lambda_1 = \mathrm{e}_{\mathrm{N}}^{(\mathrm{Al})} = -0.071 \pm 0.03$

$\lambda_2 = \mathrm{r}_{\mathrm{N}}^{(\mathrm{Al})} = 0.0015 \pm 0.0014$

$\lambda_2 = \mathrm{r}_{\mathrm{Al}}^{(\mathrm{N})} = -141.8 \pm 24.96$

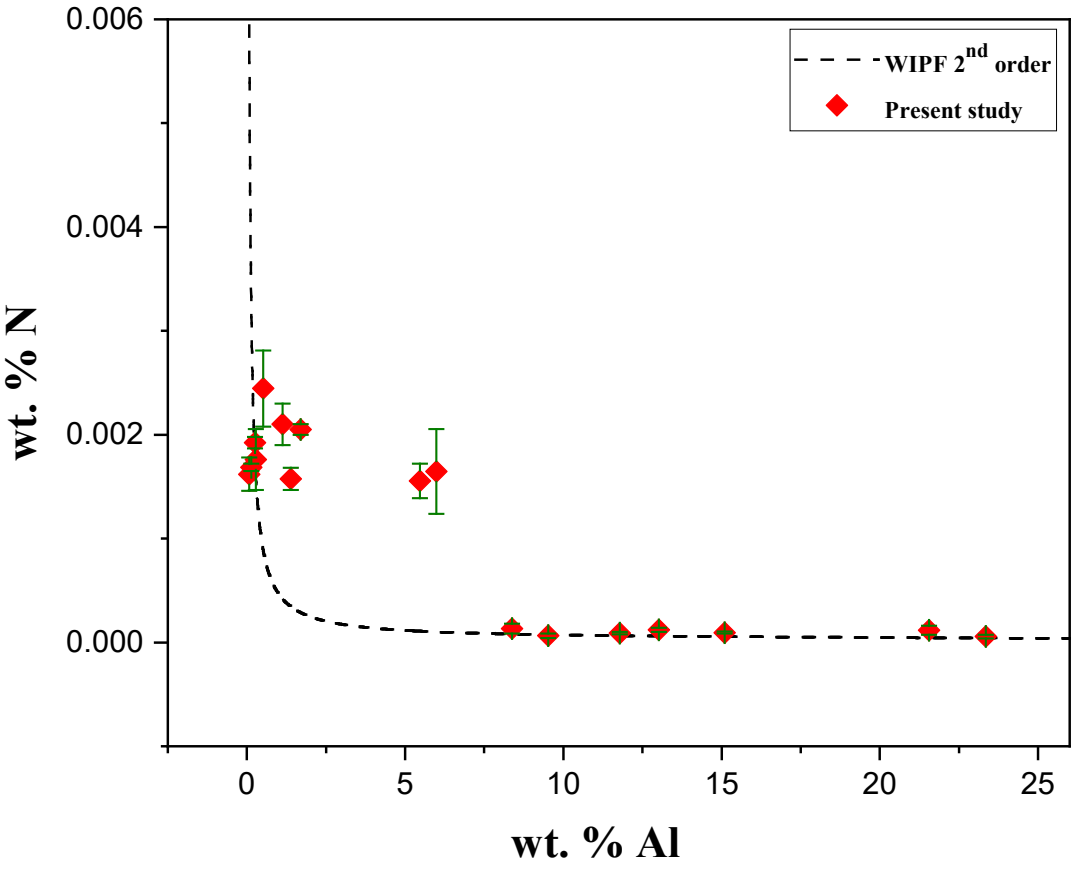

Figure 3 – Solubility of nitrogen at varying concentration of Al in steels. Symbols denote the experimental data and the solid line represent the curve obtained by WIPF 2nd order formalism

The value of $\log K$ obtained in the present study is -3.355 using WIPF 2nd order. The values of $\log K$ obtained by the different researchers at 1873 K are -1.361 (Evans and Pehlke, 1964), -1.606 (Adachi, Morita and Wada, 1966), -1.267 (Wada and Pehlke, 1978) and -1.44 (Kim *et al*, 2007) while the values of 1st order interaction parameter $e_N^{(Al)}$ have been reported by some researchers as positive and others have reported its value as negative. The value of $e_N^{(Al)}$ at 1873 K as reported by different researchers are 0.017 (Kim *et al*, 2007), -0.028 (Evans and Pehlke, 1964) -0.025 (Adachi, Morita and Wada, 1966), -0.023 (Wada and Pehlke, 1978). The absolute value of $\log K$ and $e_N^{(Al)}$ in the present study is roughly three times greater than the values obtained by previous researchers. The present experiments were nitrogen deficient and aluminium concentration was much higher for most of the samples.

3. (b) Inclusion analysis

The top central portion was examined under SEM for inclusion analysis. A cuboidal sample from two different experiments containing 5.985 and 11.78 wt.% of aluminium were extracted close to the top region. The samples preparation is explained in the section Experimental Methodology. SEM-EDS investigation revealed the presence of dual-phase inclusions in the samples comprising of nearly spherical alumina in the center and AlN at the periphery.

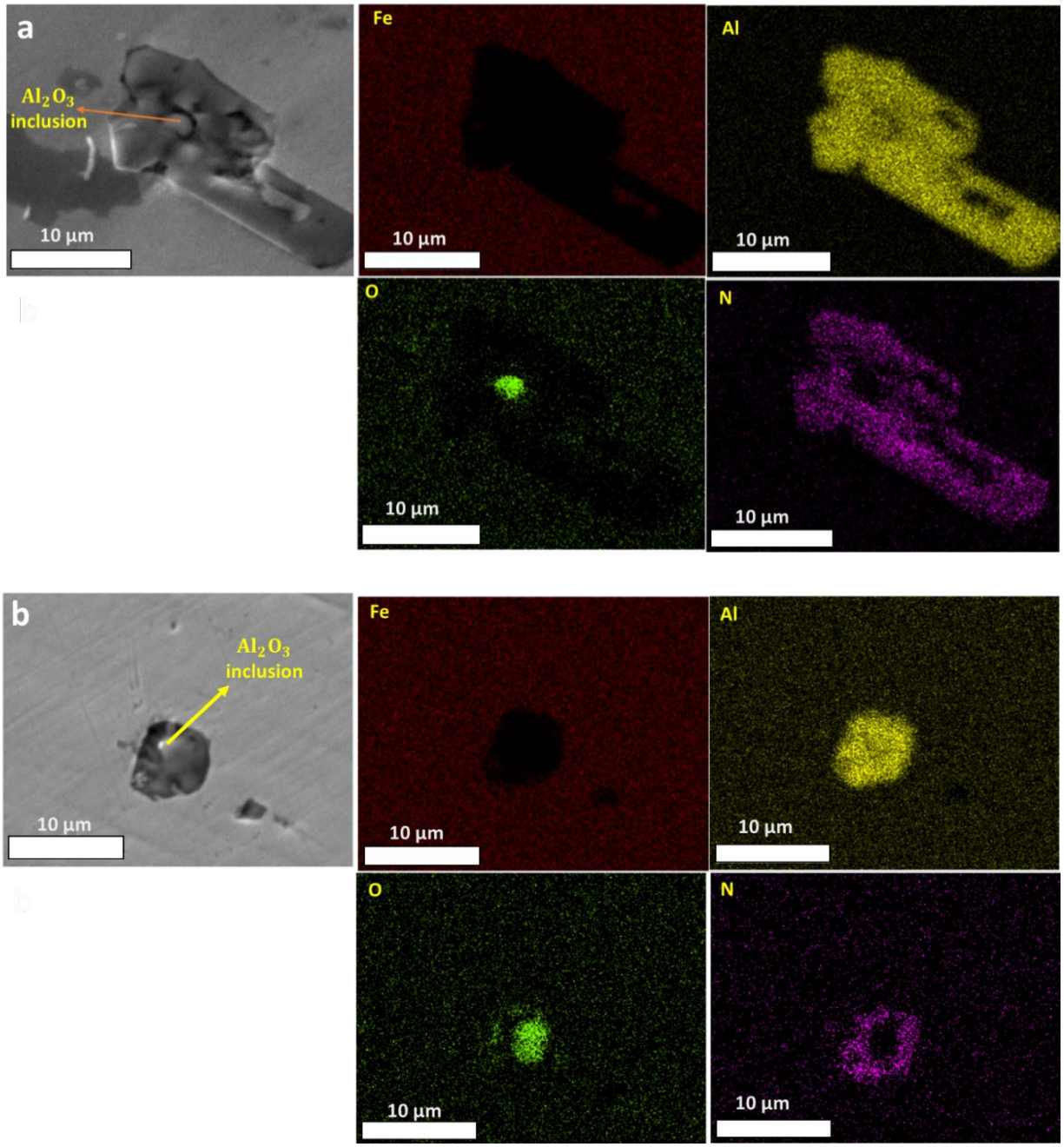

Figure 4 - BSE image and elemental mapping of aluminium nitride containing Al_2O_3 inclusion in its core while as AlN occupies the peripheral region (a) sample with (Al -5.985 wt.% Al) (b) sample with (Al-11.78 wt.% Al)

Figure 4 shows dual phase inclusions (a) with a ripsaw morphology and (b) globular shape with a composition AlN at the outer periphery and Al_2O_3 in the centres. As mentioned by Alba (2021) that AlN is not stable at 1873 K at low nitrogen content. The aluminium nitride therefore grows over the pre-existing alumina inclusions. These alumina inclusions act as nucleating sites for nitrides to grow as can be seen in **Figure 4**. The EDS of the oxide inclusion located in the core of **Figure 4. (a)** showed pure alumina.

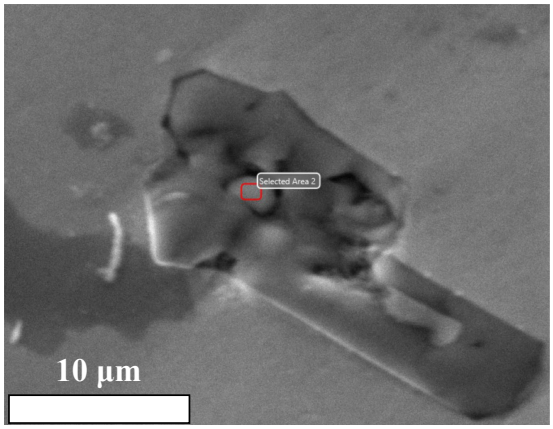

Element	Weight. %	Atomic %
O	50.8	63.5
Al	49.2	36.5

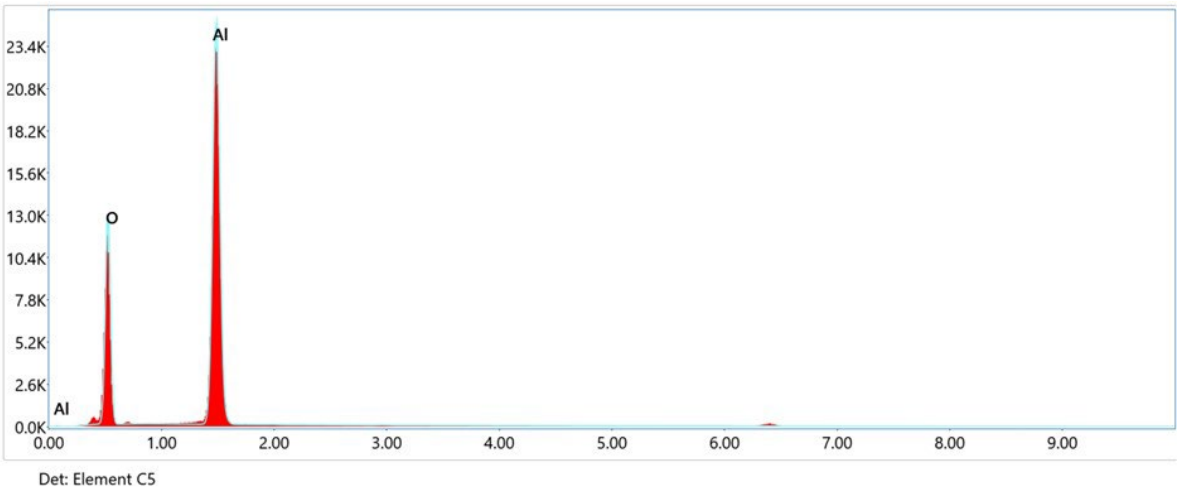

Figure 5 - EDS of the centered alumina inclusion (located in the core) of Figure 4 (a)

Alba (2021) and Guo *et al* (2023) obtained similar results. Using SEM analysis, they found out that AlN inclusions grow on the alumina inclusions. A heterogenous nucleation site thus promotes the growth of aluminium nitrides. Willems *et al.* (1992) found out that single phase Al-O-N inclusion is stable only above 1923 K and dissociates into alumina and alumina nitride below this temperature. Nucleation of one type of inclusion over the other requires closeness in lattice fit. Bramfitt (1970) propounded that any nucleating site can be effective for a different

inclusion to grow on its surface if lattice disregistry between the nucleating inclusion and substrate is less than 12%. The lattice disregistry between (0001) AlN plane and (0001) alumina plane is about 12% which indicates that AlN could grow on alumina substrate (Dovidenko *et al*, 1996). Presence of more oxygen in the melt decreases the contact angle between inclusion and steel. This can affect the size of inclusions as well. The relationship between contact angle (θ) and weight percentage of oxygen (Kawai and Shiraishi, 1988) can be given as

$$\theta = 132 - 6.3\ln(1 + 400(\text{wt.}\%\text{O})) \quad (12)$$

Since equilibrium concentration of oxygen in the melt is dependent on aluminium, so contact angle will also depend on aluminium. Further, aluminium will have its own individual effect on the surface tension of melt. The average size of aluminium nitride reported by Hsiao (1958) was in the range of 10-80 nm. However, aluminium concentration was in the deoxidation range (850 ppm). More oxygen in the melt decreases the contact angle of inclusions with steel thus promoting smaller sizes of inclusions. In the present experiments, oxygen concentration was in the 10-ppm range so the contact angle of alumina inclusions was higher (130-136°). This clearly indicates the tendency of alumina inclusions to agglomerate and minimize contact with the steel.

It can be envisaged that the agglomerate was the outcome of accumulation of various particle sizes after the acid dissolution of the top surface of solidified ingot as filtrate residue. Such inclusion clusters were not found in polished surface of CB sample during SEM analysis. The elemental mapping was also done to confirm the presence of elements (Al, O and N).

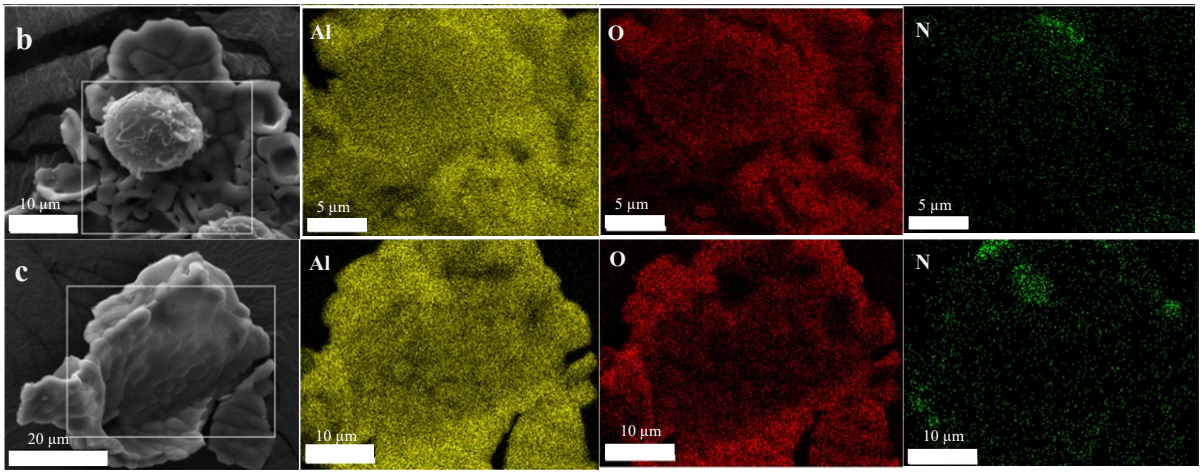

Figure 6 - The elemental mapping of the extracted inclusions (taken from the top portion of ingot as shown in **Figure 2**) shows presence of Al and O with minute distribution of nitrogen

Pure alumina inclusions were observed at the top surface after examining the filtrate using SEM-EDS (Scanning Electron Microscopy with Energy Dispersive X-ray Spectroscopy). **Figure 6** illustrate a sparse distribution of nitrogen in the inclusions. These observations confirm that any nitrogen contamination from the atmosphere can be ruled out completely.

Conclusions

1. The examination of nitrogen solubility at various aluminum concentrations in steels was conducted within a controlled atmosphere of pure argon, as opposed to nitrogen atmosphere. The initial nitrogen concentration was notably low.
2. Increase in aluminium led to the decrease in the nitrogen levels, which was not prominent in low aluminium concentration range. However, in samples containing more than 8 wt.% of aluminum, the nitrogen levels consistently remained around 1 ppm for all samples.
3. Using 2nd order Wagner's interaction parameter formalism, the value of $\log K$ was found to be -3.355 while the first cross order interaction parameter $e_N^{(Al)}$ was found to be -0.071. The value of 2nd order interaction parameters $r_N^{(Al)}$ and $r_{Al}^{(N)}$ were found to be 0.0015 and -141.79 respectively.
4. SEM-EDS analysis revealed the presence of nitride inclusions, which exhibited a tendency to grow over pre-existing alumina inclusions, forming dual-phase inclusions.

Acknowledgements

The authors express their appreciation to IIT Bombay for the resources made available for the experimental work conducted in the current study. The financial support provided by (1) Industrial Research and Consultancy Center (IRCC) IIT Bombay, Mumbai and (2) Science and Engineering Research Board (SERB), Department of Science and Technology, Government of India is also gratefully acknowledged.

References

Adachi, A, Morita, Z and Wada, J, 1966, *The 19th Comm. (Reaction), Japan Soc. Promotion Sci. (JSPS)*, Rep. No. 19-8134.

Alba, M, 2021. Experimental investigation on inclusions in medium manganese steels and high manganese steels, PhD thesis, McMaster University, Hamilton.

Beeghly, H F, 1949. Behavior of nitrogen and some of its compounds in steel, *Analyt. Chem.*, 21: 1513−1519.

Bramfitt, B L, 1970. The effect of carbide and nitride additions on the heterogeneous nucleation behavior of liquid iron, *Metall Trans*., 1: 1987-1995.

Dekkers, R, Blanpain, B and Wollants, P, 2003. Crystal Growth in Liquid Steel during Secondary Metallurgy, *Met. Trans. B*, 34: 161-171.

Dovidenko, K, Oktyabrsky, S, Narayan J and Razeghi, M, 1996. Aluminium nitride films on different orientations of sapphire and silicon, *J. Appl. Phys.*, 79: 2439–2445.

Duan, H, Ren, Y, Thomas, B G and Zhang, L, 2019. Agglomeration of solid inclusions in molten steel, *Met. Trans. B*., 50: 36-41.

Evans D B and Pehlke, R D, 1964. The Aluminium nitrogen equilibrium in liquid Iron, *Trans. TMS-AIME*, 230: 1651–1656.

Guo, Y, Cao, L, Wang G and Liu C, 2023, Precipitation behaviors of AlN inclusion in high-Al Steel, *Metall. Mater. Trans. B*, 54: 275–286.

Hsiao, C C, 1958. Fine Aluminium Nitride Precipitates in Steel, *Nature*, 181: 1527-1528.

Ishfaq, M and Pande, M M, 2024. Establishing Aluminum-Oxygen (Al-O) Equilibria in Liquid Iron at 1873 K: An Experimental Study and Thermodynamic Analysis, *Metall. Mater. Trans. B*, https://doi.org/10.1007/s11663-024-03054-w.

Ishii, F, Ban-ya, S and Fuwa, T, 1982. Solubility of nitrogen in liquid iron alloys, *Testu-to-Hagane*, 68: 1551-1559.

Kang, Y, Thunman, M, Sichen, D, Morohoshi, T, Mizukami K and Morita, K, 2009. *ISIJ Int*., 49: 1483-1489.

Kawai Y and Shiraishi, Y, 1988, *Handbook of Physico-chemical Properties at High Temperatures*, *ISIJ*, pp. 158.

Kim, W Y, Kang, J G, Park, C H, Lee, J B and Pak, J J, 2007. Thermodynamics of aluminum, nitrogen and AlN formation in liquid iron, *ISIJ Int*., 47: 945-954.

Lupis, C H P, 1983. *Chemical Thermodynamics of Materials* (North Holland, New York).

Paek, M K, Jang, J M, Do, K H and Pak, J J, 2013. Nitrogen solubility in high manganese-aluminium alloyed liquid steels, *Met. Mater. Int*., 19: 1077-1081.

Paek, M K, Jang, J M, Kang, Y B and Pak, J J, 2015. *Metall. Mater. Trans. B*, 46: 1826-1836.

Pehlke, R D and Elliott, J F, 1960. Solubility of nitrogen in liquid iron alloys, 1. Thermodynamics, *Trans Met. Soc. AIME*, 218: 1088-1101.

Sieverts, A and Zapf, G, 1935. Iron and nitrogen, *Zeitschrift f. Phys. Chemie*, 172: 314-315.

Sigworth, G K and Elliott, J F, 1974. The Thermodynamics of Liquid Dilute Iron Alloys 1974. *Metal Science*, 8: 298-310.

Turkdogan, E T, 1980. Physical Chemistry of High Temperature Technology, pp. 81(Academic Press: New York).

Wada, H and Pehlke R D, 1977. Nitrogen solution and titanium nitride precipitation in liquid Fe-Cr-Ni alloys, *Met. Trans. B*, 8: 443-450.

Wada W and Pehlke, R D, 1978. Nitrogen solubility and aluminum nitride precipitation in liquid iron, Fe-Cr, Fe-Cr-Ni, and Fe-Cr-Ni-Mo alloys, *Met. Trans. B*, 1978, 9: 441–448.

Willems, H X, Hendrix, M M R M, With, G de and Metselaar, R, 1992. Thermodynamics of Alon II: Phase relations, *Journal of the Eu. Cer. Soc*., 10: 339-346.